Mechanisms and Kinetics of Methane Thermal Conversion in a Syngas

ARTICLE *in* INDUSTRIAL & ENGINEERING CHEMISTRY RESEARCH · JUNE 2009

Impact Factor: 2.59 · DOI: 10.1021/ie900343b

7 AUTHORS, INCLUDING:

Anthony Dufour

French National Centre for Scientific Resea…

58 PUBLICATIONS **746** CITATIONS

SEE PROFILE

Mechanisms and Kinetics of Methane Thermal Conversion in a Syngas

Anthony Dufour,*,†,‡ Sylvie Valin,§ Pierre Castelli,§ Sébastien Thiery,§ Guillaume Boissonnet,§ André Zoulalian,⊥ and Pierre-Alexandre Glaude||

Research & Development Division, Gaz de France, 361 avenue du Président Wilson, BP 33, F-93211 Saint-Denis-la-Plaine cedex, France, CEA, DEN, 17 rue des Martyrs, F-38054 Grenoble, France, Faculté des Sciences & Techniques, LERMaB, Nancy-Université, INRA, BP 239, F-54506 Vandoeuvre lès Nancy cedex, France, and DCPR, Nancy-Université, CNRS, 1 rue Grandville, B.P. 20451 F-54001 Nancy cedex, France

In order to optimize H_2 and CO production from biomass gasification, the thermal decomposition of methane in a reconstituted syngas was investigated in a tubular reactor at 130 kPa, for a gas residence time of 2 s and as a function of temperature (1000−1400 °C), CH_4 (7, 14%), H_2 (16, 32%), and H_2O (15, 25, 30%) initial mole fractions. H_2 showed an inhibiting effect on CH_4 conversion whereas H_2O had few effects. Three detailed elementary mechanisms were used to predict the methane conversion rate and to identify the key reaction pathways. Flow rate analyses showed that carbon oxidation occurs mainly by addition of OH radicals on C_2 compounds. OH radicals are mainly produced by CO_2 ($CO_2 + H = CO + OH$). The inhibiting role of H_2 on CH_4 conversion is explained by a competition between the OH radicals consumption channels ($H_2 + OH = H_2O + H$). The competition between thermal conversion of methane and reforming of unsaturated C_2 explains the soot formation.

1. Introduction

Biomass gasification is a promising route of gaseous and liquid fuels production such as CH_4, H_2, Fischer−Tropsch diesel, or methanol. Biomass gasification processes produce a syngas mainly composed of CO, H_2, H_2O, CO_2, CH_4, and C_2 compounds and tar. CH_4 conversion into H_2 and CO has been identified as one of the main key points to optimize H_2 recovery and the overall energetic efficiency of the H_2 production from biomass gasification.[1,2] Methane is formed during biomass pyrolysis and tar cracking, and it roughly represents 30 mol % of the hydrogen element contained in the products of wood pyrolysis at 800 °C (including permanent gases, char, water, and tar).[3]

The most studied methane up-grading technology is catalytic gas conditioning. Metal based catalysts and especially Ni-based catalysts have been extensively studied.[4−6] However, they are prone to deactivation due to coke accumulation on the catalytic surface and to sulfur poisoning, when used to up-grade a real biomass syngas.[7−9] Other alternative strategies for methane reforming could be the use of carbon-based catalysts such as wood char[10] or thermal decomposition (without any catalysts).

Thermal decomposition of methane was reviewed by Khan et al.,[11] Back and Back,[12] and Billaud et al.[13] Pyrolysis of pure CH_4 (diluted in an inert gas) was extensively studied in a wide range of conditions.[14−26] However, these works focused most of the time on C_2H_2 production[17,18,20,21,23,25] or on carbon vapor deposition.[19,22]

Numerous studies dealt with the effect of H_2[15,17,18,23−26] or H_2O[17,24] addition on CH_4 thermal decomposition mainly in order to maximize the C_2H_2 selectivity. The effect of CO_2 addition was studied, to our knowledge, exclusively in the presence of O_2.[27,28] Moreover, numerous detailed mechanisms validated for an extensive range of CH_4 combustion conditions were developed.[29−35]

The conversion of CH_4 in presence of H_2, CO_2, H_2O, and CO with a composition representative of a biomass pyrolysis gas has only been studied, to our knowledge, by Jönsson.[36] Jönsson investigated thermal reactions at temperatures lower than 1250 °C. Methane conversions lower than 60% were achieved, and no kinetic data were derived.

To our knowledge, in spite of the numerous studies on CH_4 conversion, no work deals with the kinetic of CH_4 thermal decomposition under the conditions of a biomass pyrolysis gas, i.e. a syngas with a high content of H_2, H_2O, CO_2, and CO. This paper provides new kinetic data on the thermal decomposition of CH_4 in such a syngas. The effects of temperature, CH_4, H_2O, and H_2 initial mole fractions on CH_4 conversion are analyzed. The main elementary reactions involved during the syngas thermal upgrading are described and discussed in order to determine the most efficient process conditions and to better understand the limitations, such as soot formation.

2. Materials and Method

The experimental apparatus was formerly presented by Valin et al.[37] with a detailed description on the facility and reactor design. Only the salient points are summarized here.

The syngas composition was controlled using mass flow rate regulators (Brooks Instrument) for each individual compound. Water was vaporized in a coiled tube before being mixed with permanent gases in a preheated zone. The nominal molar gas composition was the following: CH_4 7%, CO 19%, CO_2 14%, H_2 16%, H_2O 25%, and N_2/Ar 7%. When the partial pressure of a compound was modified, the partial pressures of other gases were kept constant by adjusting the nitrogen flow.

The preheated gas was injected in an alumina tubular reactor (838 mm length and 70 mm diameter). The reactor was specifically designed to study the reforming of hydrocarbons such as methane and tar at high temperatures between 1000 and 1500 °C.[37] The absolute pressure in the reactor was approximately 130 kPa to make up for the pressure drops, the

* To whom correspondence should be addressed. E-mail: anthony.dufour@yahoo.fr.
† Gaz de France.
‡ Present adress: LSGC, Nancy-Université, CNRS, 1 rue Grandville BP 451 54001 Nancy cedex, France.
§ CEA, DEN.
⊥ Faculté des Sciences & Techniques, LERMaB, Nancy-Université, INRA.
|| DCPR, Nancy-Université, CNRS.

10.1021/ie900343b CCC: $40.75
Published on Web 06/22/2009

Table 1. Experimental Conditions[a]

	mole fraction (%) (balance N_2/Ar)				
temperature (°C)	CH_4	H_2O	H_2	CO	CO_2
992−1372 (1187)	7−14 (7)	15−30 (25)	16−32 (16)	19	14

[a] Residence time $\tau = 2$ s, total pressure 130 kPa, standard conditions in parentheses.

outlet of the reactor being at atmospheric pressure. Temperature was monitored by two type B thermocouples. The gas residence time distribution in the tubular reactor was characterized by unsteady 3D computational fluid dynamics (CFD) by using the Fluent code.[37] The 3D simulations were performed under the laminar assumption ($Re_{max} = 900$). The axial dispersion coefficient was determined by using oxygen as a tracer in the simulations.[37] The Peclet number is close to 40 for our reactor, which is very close to the plug-flow assumption condition ($Pe > 50$). Moreover, gas composition evolution at the outlet of the reactor was simulated and compared for 3D (laminar assumption) and 1D (plug-flow assumption) simulations, with the same chemical mechanism. The differences between the two simulated gas compositions are very small from 0.2 s gas residence time.[37] Consequently, the plug-flow assumption is justified for our experimental conditions. Nevertheless, an uncertainty of the residence time remains. The relative errors of gas residence time measurements were estimated at ±0.1 s.[37] The sensitivity of our results on the uncertainty of the residence time is evaluated in section 5.2.1. The residence time was kept constant as the reactor temperature was changed by adjusting the total flow rate at the entrance of the reactor.

The accuracy of temperature measurement was previously discussed.[37] The relative errors of temperature were estimated at ±15 °C.

At the reactor outlet, soot was separated from the gas phase by four filters heated at 200 °C. Water was condensed in two cold traps (20 and 0 °C) and continuously quantified. The dry gas mass flow rate was measured by a Coriolis flow meter (Brooks). The gas composition was then analyzed with a micro gas chromatograph equipped with three columns (two 5A molecular sieves, with argon and helium as different carrier gases, and one Poraplot Q with helium as carrier gas) and three thermal conductivity detectors (Varian). The relative errors of the gas fractions were estimated at ±5% except for H_2 and H_2O. The relative error of H_2O lies between −10% and 0%. The absolute error of the H_2 mole fraction analysis lies between −2% and 0%. These errors were justified in ref 37.

The analytical system thus allows the determination of the molar flow rate of water and gaseous products. For most tests, more than 94% of the carbon was measured in the gas at the exit.[37]

The conversion (X_i) or production (Y_i) degree of a compound, i, was then defined as

$$X_i = \frac{F_{i,\text{in}} - F_{i,\text{out}}}{F_{i,\text{in}}} \quad (1)$$

$$Y_i = \frac{F_{i,\text{out}} - F_{i,\text{in}}}{F_{i,\text{in}}} \quad (2)$$

with F_i, the molar flow rate (mol s^{-1}) at the inlet ($F_{i,\text{in}}$) or at the outlet ($F_{i,\text{out}}$) of the reactor.

The experimental conditions are given in Table 1.

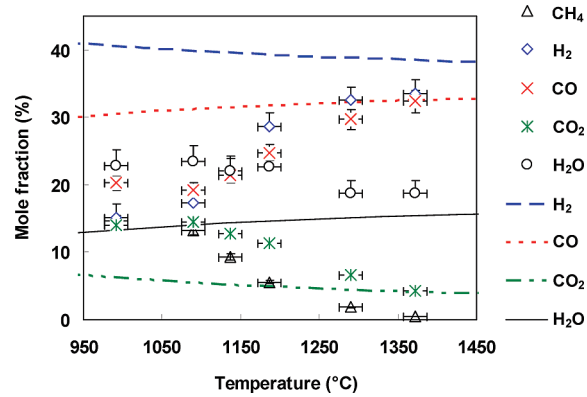

Figure 1. Evolution of the gas composition at the reactor outlet (points) and at thermodynamic equilibrium (lines) as a function of temperature, $\tau = 2$ s: inlet gas composition CH_4/14%, H_2O/25%, CO/19%, H_2/16%, CO_2/14%, Ar and N_2 QS.

3. Experimental Results

3.1. Comparison between Experimental Gas Composition and Theoretical Composition at Thermodynamic Equilibrium. It is of great interest to compare the experimental gas compositions to ones at thermodynamic equilibrium in order to understand how either the thermodynamic equilibrium or the kinetic rates control the gas phase chemistry. The evolution of gas composition at the reactor outlet and at thermodynamic equilibrium (determined with the Gaseq equilibrium program[38]) is presented in Figure 1.

With increasing temperature, the experimental H_2 and CO mole fractions increase whereas the H_2O, CO_2, and CH_4 mole fractions decrease. A methane conversion close to 100% is obtained at 1370 °C. The H_2O mole fraction decreases less than that of CO_2 (see Figure 1). At 1372 °C, H_2 mole fractions of 25 and 33% were achieved for initial CH_4 mole fractions of 7 (results not shown) and 14%, respectively. Carbon atoms from CH_4 are mainly converted to CO. The H_2/CO ratio is close to 1 for both CH_4 mole fractions.

The CH_4 mole fraction at equilibrium is not represented in Figure 1 because calculations predict a CH_4 mole fraction below 1 ppmv for all temperatures. The experimental CO and CO_2 mole fractions are close to the one determined at thermodynamic equilibrium above 1300 °C. H_2 and H_2O do not seem to reach thermodynamic equilibrium below 1400 °C. This former observation and the detection of CH_4 and soot at the outlet of the reactor evidence that the reactive system does not reach thermodynamic equilibrium under our conditions. Consequently, a kinetic approach is suitable to describe the evolution of the gas composition, even at the highest temperatures.

3.2. Conversion and Production Degrees. A significant H_2 production rate of 150% is achieved at 1370 °C (Figure 2). H_2 is mainly produced from CH_4 conversion and only a small part of H_2 comes from H_2O conversion. Indeed, little H_2O conversion is observed even at 1290 °C (conversion rate below 25% at 1187 °C). CO_2 conversion reaches 65% at 1370 °C. The detailed reactions which are involved in these gas conversions are discussed later.

3.3. Experimental Results of CH_4 Conversion. 3.3.1. Effect of Temperature and Initial CH_4 Mole Fraction. CH_4 conversion runs from 5% at 992 °C to 95% at 1372 °C (Figure 3). The initial CH_4 mole fraction has a sensitive effect for its conversion, between 1137 and 1290 °C. At 1137 °C, CH_4 conversion is 21 and 36% for 7 and 14 mol % CH_4 initial mole fractions, respectively.

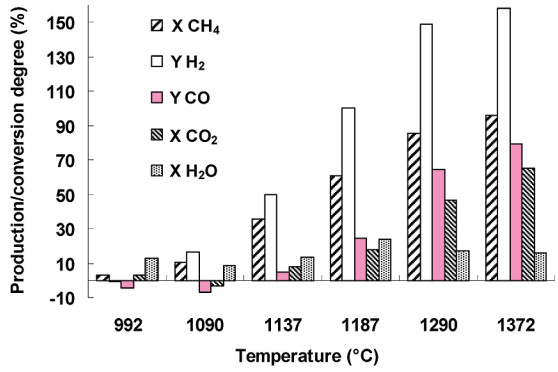

Figure 2. Evolution of the production and conversion degrees as a function of temperature $\tau = 2$ s, inlet gas composition CH_4/14%, H_2O/25%, CO/19%, H_2/16%, CO_2/14%, Ar and N_2 QS.

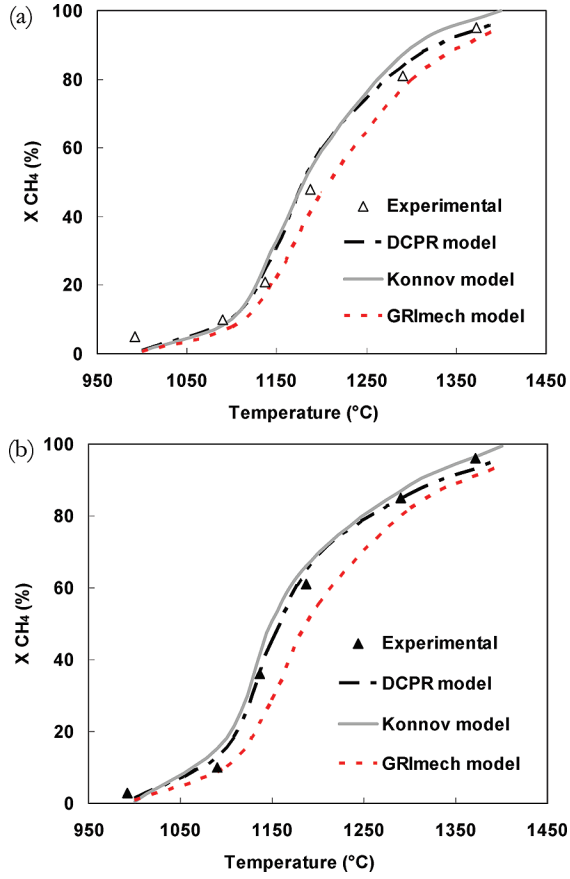

Figure 3. Effect of temperature and initial CH_4 mole fraction on CH_4 conversion ($\tau = 2$ s), initial CH_4 mole fraction of 7 (a) and 14% (b).

The determined CH_4 conversion cannot be compared with kinetic data from the literature as no reference, to our knowledge, dealt with CH_4 conversion in similar conditions (temperature, initial gas composition, and gas residence time). The experimental CH_4 conversion rates are more extensively discussed later and compared to the predictions of detailed mechanisms (section 5).

3.3.2. Effect of H_2 and H_2O on CH_4 Conversion. Figure 4 presents the effect of H_2 initial mole fraction on CH_4 conversion. Experimental results put in evidence the inhibiting effect of H_2 on CH_4 conversion. This finding is in agreement with many former works.[15,18,36] As the H_2 initial mole fraction increases from 16 to 32 vol %, the experimental CH_4 conversion rate decreases from about 50 to 30%.

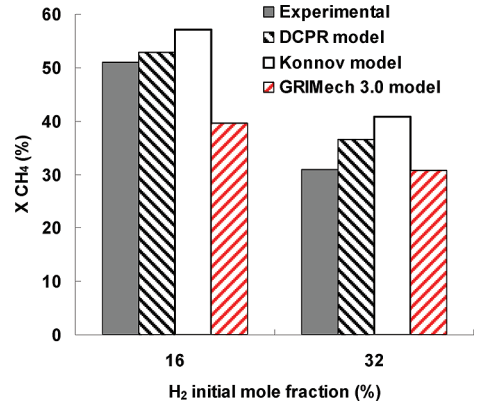

Figure 4. Effect of H_2 initial mole fraction on CH_4 conversion (standard conditions).

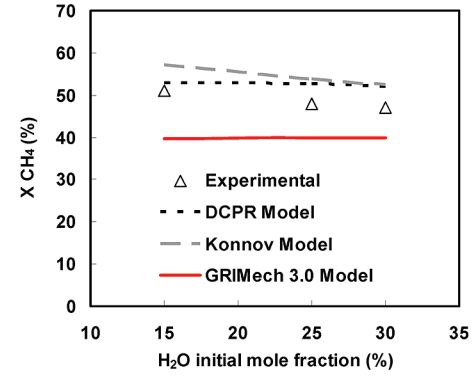

Figure 5. Effect of H_2O initial mole fraction on CH_4 conversion (standard conditions).

From 15 to 30% initial mole fraction, H_2O has only a slight chemical effect on CH_4 conversion at 1187 °C and for a gas residence time of 2 s (see Figure 5). Moreover, a slight inhibiting effect of H_2O on CH_4 conversion can be noticed.

4. Kinetics of the Apparent CH_4 Decomposition Reaction

The apparent CH_4 decomposition rate in the reactor, r_{CH_4}, was described by the following equation:

$$r_{CH_4} = kP_{CH_4}{}^{m}P_{H_2}{}^{n}P_{H_2O}{}^{p} \quad (3)$$

with r_{CH_4} (mole m^{-3} s^{-1}), the reaction rate of CH_4 decomposition, P_i (atm), the average partial pressure of each compound, i, between the inlet and the outlet of the reactor, m, n, and p, the apparent reaction orders of CH_4, H_2, and H_2O, respectively, and k (mole m^{-3} s^{-1} $atm^{-(m+n+p)}$), the apparent rate constant of CH_4 decomposition.

The rate constant of CH_4 decomposition was assumed to follow an Arrhenius law, as

$$k = k_o \exp \frac{-E}{RT}$$

with k_o (mole m^{-3} s^{-1} $atm^{-(m+n+p)}$), the pre-exponential factor, E (J mol^{-1}), the activation energy, R, the universal gas constant ($R = 8.314$ J mol^{-1} K^{-1}), and T (K), the temperature.

The CH_4 concentration profile along the reactor length was not known. Consequently, the CH_4 decomposition rate could not be integrated for each elemental volume of the reactor. An average CH_4 decomposition rate was calculated, as

$$r_{CH_4} = \frac{F_{CH_4 in} - F_{CH_4 out}}{V} = \frac{XP_{0CH_4}}{RT\tau} \quad (4)$$

with: P_{0CH_4} (atm), the CH_4 partial pressure at the inlet of the reactor, X, the CH_4 conversion rate, R, the universal gas constant (8.2×10^{-5} m^3 atm mol^{-1} K^{-1}), T (K), the reactor temperature (K), and τ (s), the gas residence time.

The calculation is only valid for a tubular reactor, for the given residence time (2 s), and range of temperature. The reaction orders m, n, and p were determined from eq 3 by systematic variation of one of the CH_4, H_2, or H_2O partial pressures at 1187 °C (experimental results presented in Figure 3−5; the partial pressures of other gases were kept invariable by adjusting the nitrogen flow). The reaction orders were the following: $m = 1.48$, $n = -0.91$, $p = -0.11$.

The rate constant, k (mole m^{-3} s^{-1} atm$^{-0.46}$), can then be calculated, for each experimental point, as

$$k = \frac{r_{CH_4}}{P_{CH_4}^{1.48} P_{H_2}^{-0.91} P_{H_2O}^{-0.11}} \quad (5)$$

The activation energy and pre-exponential factor were determined from experiments at different temperatures (Figure 3).

The CH_4 decomposition rate can be described for our experimental conditions (summarized in Table 1) by the following relationship:

$$r_{CH_4} = \left(4.7 \times 10^7 \exp \frac{-211000}{RT}\right) P_{CH_4}^{1.48} P_{H_2}^{-0.91} P_{H_2O}^{-0.11}$$

The value of the activation energy (211 kJ mol^{-1}) is lower than the one determined for instance by Bruggert et al.[22] or Holmen et al.[23] (400 kJ mol^{-1}) for the decomposition of pure CH_4, with a different gas composition and lower CH_4 conversion rates than in our case.

Due to the higher CH_4 conversion rates investigated in this work, the initiation reactions, which are characterized by a higher activation energy, become minor reactions whereas the propagation reactions decrease the apparent activation energy. Moreover, a lower apparent activation energy is determined in our case due to the consideration of an average methane conversion. Indeed, the determined conversion rate, which is an average along the reactor, is lower than the initial value at the entrance of the reactor and especially when the temperature increases with a constant gas residence time. Consequently, the effect of temperature on methane conversion rate and the activation energy is lowered. Moreover, as it will be shown hereafter, H_2, H_2O, CO, and CO_2 have a kinetic effect on methane conversion.

5. Simulation of CH_4 Decomposition with Detailed Mechanisms

5.1. Presentation of the Mechanisms. Global kinetic models (as developed in the previous section) are generally only validated for a short-range of experimental conditions and do not describe the elementary pathways of CH_4 decomposition. To overcome these drawbacks, many detailed mechanisms were developed especially for the combustion of methane.[29−35] The aim of this section is not to develop a new mechanism but to compare some previously developed mechanisms and to identify the main elementary reactions and the most sensible ones for CH_4 decomposition in our operating conditions.

For this purpose, three detailed mechanisms were used and compared: the DPCR (mechanism developed at Département de Chimie Physique des Réactions, CNRS, Nancy, France), Konnov's, and GRImech3.0 mechanisms. These mechanisms were validated for an extensive range of CH_4 (and some heavier hydrocarbons as described hereafter) combustion conditions. The sensitive reactions in our experimental conditions will be different to that in combustion due to high concentrations of CO and H_2 (reduction conditions) and slow oxidation rates (CO_2, H_2O). Their kinetic constants may be known less accurately. Nevertheless, these elementary mechanisms could be valid to predict the reactivity of CH_4 and some other species in our experimental conditions as well.

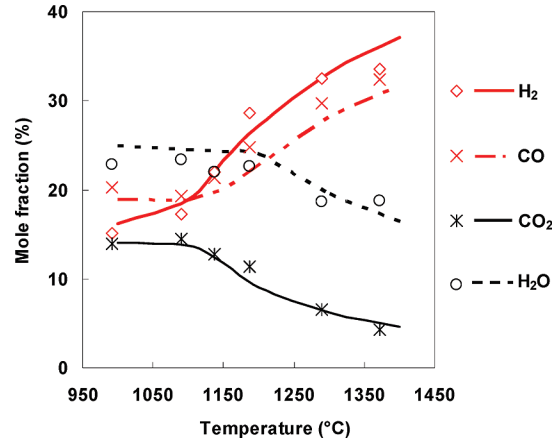

Figure 6. Simulation (DCPR mechanism) and experimental results of the gas composition as a function of temperature. Points are experiments, and lines, simulations. $\tau = 2$ s, initial gas composition CH_4/14%, H_2O/25%, CO/19%, H_2/16%, CO_2/14%, Ar and N_2 QS.

The DCPR mechanism was previously developed by Barbé et al.[30] and then updated by Fournet et al.,[39] Belmekki et al.,[40] and Gueniche et al.[41] The reaction base includes 116 species and 811 elementary reactions. It was validated for the formation and oxidation of CH_4, C_2H_6, C_3-C_4 unsaturated hydrocarbons and benzene. This mechanism is the only one of the three ones investigated in this paper, which takes into account the benzene formation and oxidation.

The Konnov's 0.5c mechanism[34] was validated for the oxidation of light hydrocarbons species from CH_4 to C_3. It includes 127 species and 1213 elementary reactions. It originates from the work of Borisov et al.[42,43] and was largely updated on the basis of recommendations of Baulch et al.[44] The Konnov's mechanism is the more systematic one of the three mechanisms because it includes all the species to C_3 and was validated in the larger range of conditions (see ref 34 for more details). The updated release 0.6 of the Konnov mechanism includes improved nitrogen chemistry, which is not of importance in the present study. This newer version will not influence the presented predictions.

The GRImech 3.0 mechanism was developed by Smith et al.[35] and was optimized for a large range of natural gas combustion conditions (see ref 35 for more details). It is a compilation of 325 elementary reactions which involve 53 species. This mechanism does not include C_3+ species except propane.

Simulations were performed using the SENKIN code from Chemkin II,[45] assuming an isothermal plug-flow reactor as justified in a previous work.[37] The SENKIN code enables to determine the gas composition evolution along the reactor length as a function of the gas residence time.

5.2. Comparison between Experimental and Simulated Results. 5.2.1. Gas Composition. Figure 6 displays the gas composition evolution (except for CH_4) simulated by the DCPR

mechanism as a function of temperature. The three mechanisms (results not shown for the other two) satisfactorily reproduce the gas composition. The sensitivity of the residence time uncertainty (2 ± 0.1 s) on predicted mole fractions was analyzed. The variation of predicted gas compositions is lower than 4% of the average outlet mole fraction for all gases and at all temperature in the range of gas residence time. For instance, at 1200 °C, which is the most sensitive temperature for methane conversion, the predicted methane conversion lies between 69.1 and 70.3% in the range of gas residence time uncertainty.

CO_2, CO, H_2, and H_2O mole fractions are well predicted by DCPR mechanism except at 1400 °C where the production of H_2 and the consumption of H_2O are slightly overpredicted. These overpredictions are higher with the Konnov's mechanism and start from 1300 °C (not shown). The Konnov's mechanism underestimates the CO_2 consumption between 1100 and 1300 °C. The GRImech mechanism underestimates H_2 and CO production and H_2O consumption between 1100 and 1300 °C. The start of the H_2O consumption is predicted by the three mechanisms at about 1200 °C whereas the start of the CO_2 consumption is predicted at about 1100 °C.

5.2.2. Effect of Temperature and Initial CH_4 Mole Fraction. Figure 3a and b displays the evolution of the experimental and simulated CH_4 conversion degrees as functions of temperature and initial CH_4 mole fraction.

The three mechanisms exhibit a very good agreement as to the effect of temperature on the CH_4 conversion rate.

The DCPR and Konnov's mechanisms give very close results, and the effects of CH_4 initial mole fraction and temperature are well predicted. The GRImech mechanism slightly underestimates the CH_4 conversion rate with a shift of 10 and 25 °C for an initial CH_4 mole fraction of 7 and 14%, respectively. This is the mechanism which predicts the least the increase in the CH_4 conversion degree when the initial CH_4 mole fraction increases.

5.2.3. Effect of Initial H_2 and H_2O Mole Fraction. Figure 4 displays the experimental and simulated CH_4 conversion degrees as a function of the initial H_2 mole fraction.

The DCPR and Konnov's mechanisms predict satisfactorily the effect of H_2 on the CH_4 conversion. The inhibiting effect of H_2 is nevertheless slightly underestimated.

The GRImech mechanism gives the closest conversion degree prediction for the highest H_2 mole fraction (32%), but the H_2 inhibiting effect is not well-predicted.

Figure 5 shows that the very low effect of H_2O on CH_4 conversion is well-represented by the three mechanisms.

6. Discussion

6.1. Flow Rate Analyses. The flow rate analyses simulated by the three mechanisms were compared in order to derive the main reaction pathways of CH_4 conversion involved in our experimental conditions and to explain the effects of H_2 and H_2O initial mole fractions on methane conversion by the means of elementary mechanisms.

Flow rate analyses were performed at 1200 °C and for a gas residence time of 1.1 s, corresponding to a CH_4 conversion degree of about 30−40%. Under these conditions, the flow rate analyses highlight the intermediate reactions occurring in the CH_4 thermal decomposition. Figures 7 and 8 display the reaction flows and the sensitive reactions in CH_4 decomposition and in H_2, H_2O, and CO production and consumption, taken from the DCPR model. The flow rate analyses performed with the two other models (Konnov and GRIMech) are not shown.

The main pathway of CH_4 consumption (DCPR model, Figure 7) is the H-abstraction by H atom to give a methyl radical and H_2 ($CH_4 + H = CH_3 + H_2$). In our conditions of intermediate CH_4 conversion, the concentration of H atoms is large and the H-abstraction is more important than the initiation reaction ($CH_4 = CH_3 + H$). This methathesis is favored by the low enthalpy of reaction. The dissociation energy of the C−H bond (440 kJ/mol) is roughly provided by the energy of the H−H bond formation (436 kJ/mol). The ratio of the H-abstraction of CH_4 by OH radicals is less than 10%. Methyl radicals then lead to the formation of ethane (C_2H_6), which is mainly dehydrogenated into ethene (C_2H_4) and then into acetylene (C_2H_2). C_2H_4 and C_2H_2 are slowly oxidized by OH radicals and lead mainly to propagation reactions involving C_2 and C_4 species. The oxidation of carbon (formation of a C−O bond) occurs mainly by the addition of OH radicals on C_2H_4 (2.1×10^{-8} mol cm^{-3} s^{-1}) and on C_2H_2 (7.5×10^{-9} mol cm^{-3} s^{-1}). The main reactions of C_2H_4 are H abstraction by H atoms and OH addition ($C_2H_4 + OH = CH_3 + HCHO$). Metathesis by OH on C_2H_4 ($C_2H_4 + OH = C_2H_3 + H_2O$) is a minor channel compared to OH addition. It represents only 13% of the total rate of these two reactions involving OH radicals with C_2H_4.

The direct oxidation by H_2O of CH_3 radicals only accounts for 30% (1.4×10^{-8} mol cm^{-3} s^{-1}) of the formation of a C−O bond.

Benzene, which is known as a soot precursor, is mainly formed from C_3H_3 radicals, which are mainly formed by C_2H_2. The formation of C_2H_2 (and then benzene and soot) is favored by the poor direct oxidation of CH_3 radicals.

H_2O is mainly produced by the reaction ($H_2 + OH = H_2O + H$), and the reactions of H_2O consumption are still slow (Figure 8). H_2 is mainly produced by the addition of H radicals on CH_4 and by dehydrogenation of C_2 species. H_2 is mainly consumed by the propagation reactions involving C_4 species, according to the DCPR model. CO and OH radicals are mainly produced by the addition of H atom to CO_2 ($CO_2 + H = CO + OH$) and are consequently not very dependent on H_2O concentration under our conditions of high concentration of CO_2. About 30% (4.7×10^{-8} mol cm^{-3} s^{-1}) of CO is produced from CHO, which is mainly formed by C_2H_4 and CH_3 oxidation.

The Konnov's model (flow rate analysis not shown) exhibits the H-abstraction to yield a methyl radical and H_2 ($CH_4 + H = CH_3 + H_2$), as the main reaction pathway of CH_4 consumption. Methyl radicals then lead to the production of C_2H_6, to C_3 and C_4 (as C_4H_6). C_2H_6 and C_4H_6 then lead to the production of C_2H_2 which is mainly oxidized by OH radicals into CO. H_2O is poorly reactive. H_2 is mainly produced from CH_4 and C_2 species. CO is mainly produced by $CO_2 + H$ and by CHO and CH_2CO conversion.

In the GRImech model, for the considered CH_4 conversion degree (∼30%), the initiation reaction ($CH_4 = CH_3 + H$) still accounts for 37% of the consumption of CH_4. The H-abstractions by H atom ($CH_4 + H = CH_3 + H_2$) and OH radicals ($CH_4 + OH = CH_3 + H_2O$) account for 51 and 11%, respectively, of the CH_4 consumption. The GRImech model mainly exhibits the following consecutive steps, with very minor other channels: $CH_4 \rightarrow CH_3 \rightarrow C_2H_6 \rightarrow C_2H_4 \rightarrow C_2H_2 \rightarrow CO$. The oxidation solely occurs by the addition of OH radicals onto C_2H_2. CO is mainly produced by the $CO_2 + H$ reaction. H_2O is not very reactive.

6.2. Comparison of the Flow Rate Analyses and of the Sensitive Reactions. In the three models, the initiation reaction is the following: $CH_4 = CH_3 + H$. Nevertheless, this reaction represents a larger flow in the GRImech model due to a lower predicted concentration of radicals. This channel appears less in the DCPR and Konnov's simulations because a larger

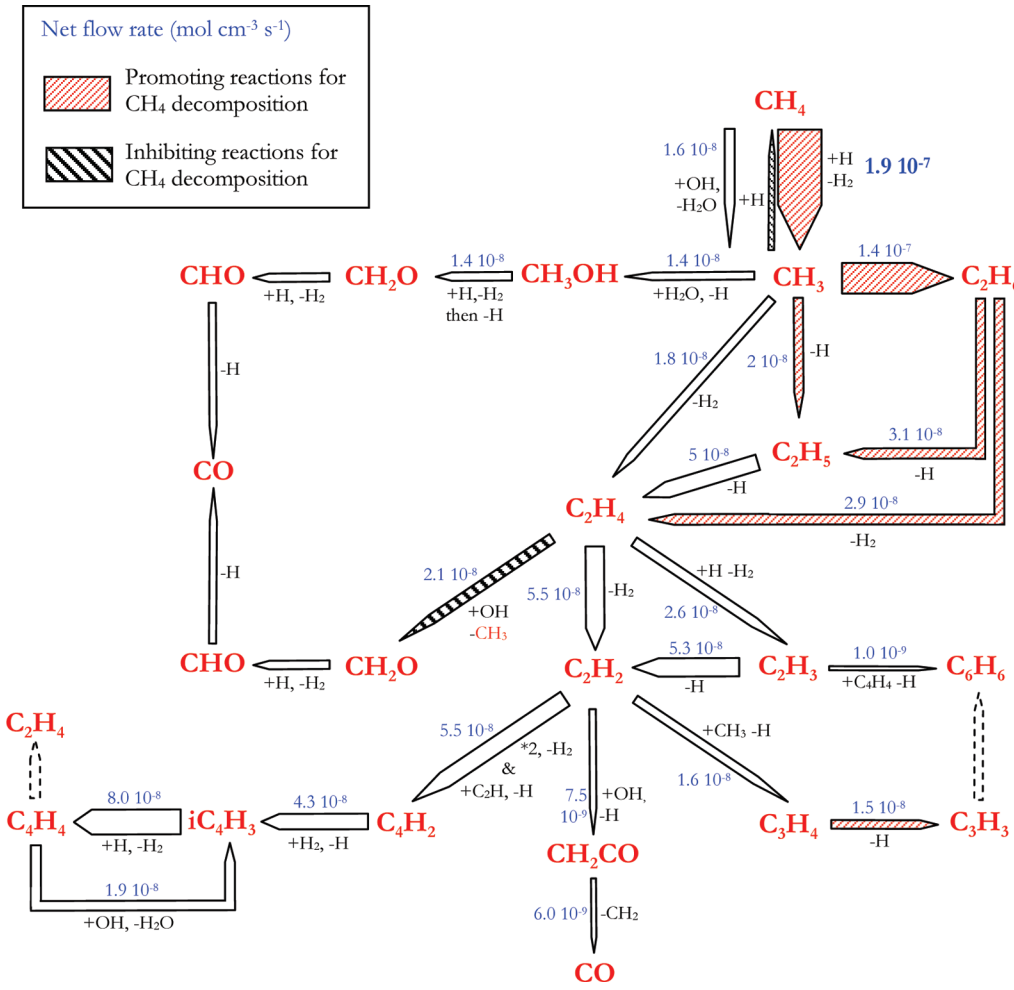

Figure 7. Flow rate analysis for the decomposition of CH_4, DCPR model, 1200 °C, τ = 1.1 s, standard initial mole fractions.

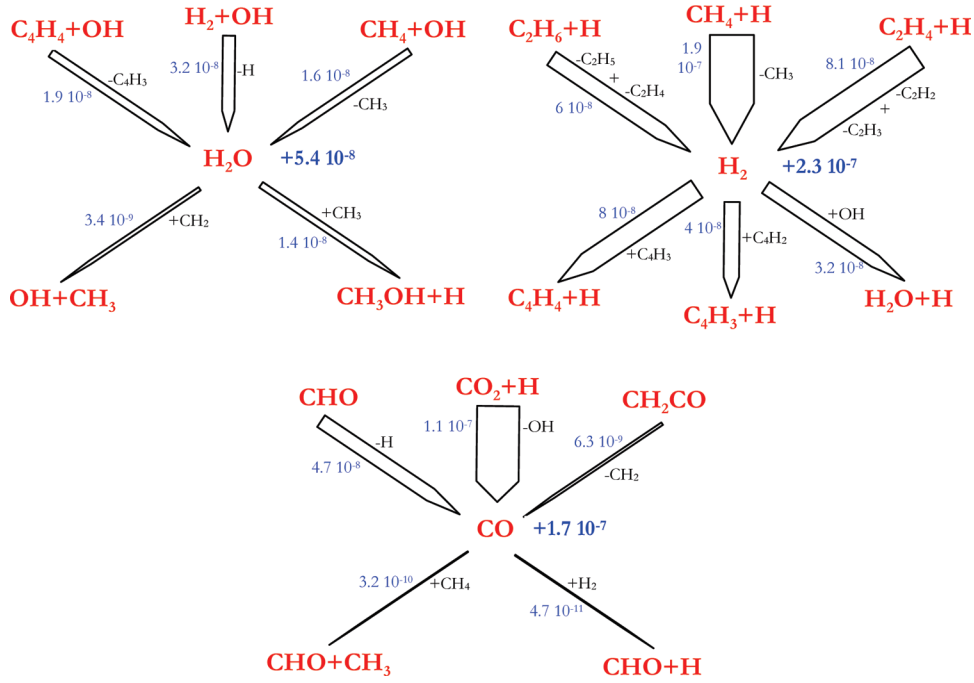

Figure 8. Flow rate analysis of the main reactions of H_2O, H_2, and CO production and consumption, DCPR model, 1200 °C, τ = 1.1 s, standard initial mole fractions.

concentration of radicals (especially H atoms) is predicted. Consequently, the propagation reactions represent the major flow rate in these two models for the investigated conditions.

In the three models, the propagation reactions involve methyl radicals, which promptly lead to the formation of C_2H_5/C_2H_6, then dehydrogenated into C_2H_4. This reaction pathway is well-

known for pure methane decomposition.[12,18] The propagation is then different for the three models.

The Konnov model exhibits propagation with C_3 species, and the DCPR model with C_4 species. C_3 and C_4 species may be overestimated because competing reactions of addition yielding heavier compounds are not included in the models.

The GRImech model exhibits the conversion of C_2H_4 solely into C_2H_2. The GRImech model does not predict the formation of species heavier than C_2 because it does not include these species (except C_3H_8 and C_3H_7). Consequently, an accumulation of C_2H_2 is predicted, which is not realistic in pyrolysis conditions.

In the three mechanisms, the propagation reactions $CO_2 + H = CO + OH$ and $H_2 + OH = H_2O + H$ exhibit important flow rates, except the former reaction for the Konnov's mechanism. The $CO_2 + H$ reaction has already been identified as the primary step responsible for the chemical effect of CO_2 in several previous study[27,28] under oxy-fuel combustion conditions but was never identified, to our knowledge, under our conditions of a syngas composition.

The three mechanisms show that the oxidation process occurs mainly by the addition of OH radicals onto C_2 species. This mechanism is similar to the oxidation of benzene by the breaking of the π bond.[41] In the three mechanisms, minor channels involve the formation of a C−O bond directly from CH_4 or CH_3 radicals.

In the three models, the promoting reactions for CH_4 decomposition are the reactions which lead to the formation and the conversion of the CH_3 radicals. The reactions of CH_3 and C_2H_6 consumption are very promoting reactions for CH_4 conversion in both DCPR and Konnov's models.

The inhibiting reactions for CH_4 conversion are the reactions of OH radicals addition on C_2H_4 (DCPR model) or on C_2H_2 (Konnov model). The sensitivity analysis of the GRImech mechanism does not exhibit inhibiting reactions.

6.3. Effect of Initial H_2 and H_2O Mole Fraction on the Reaction Pathways. The flow rate analyses were performed for the three models at 1200 °C, 1.1 s gas residence time, initial H_2 mole fraction of 32% (not shown). The effect of H_2 on the reaction pathways was studied by the comparison of the flow rate analyses performed for the two different H_2 initial mole fractions (16 vol %, displayed in Figures 7 and 8 for the DCPR model, and 32 vol %).

In the three mechanisms, at higher H_2 mole fraction, the consumption of OH radicals by the $H_2 + OH$ reaction is favored. OH radicals become less available for the C_2 oxidation reactions, which explains the inhibiting effect of H_2 on CH_4 conversion.

Nevertheless, the flow rate of the ($C_2H_4 + OH = CH_2O + CH_3$) reaction (inhibiting reaction in the DCPR mechanism) is increased in the DCPR and Konnov's mechanisms, because the C_2H_4 production is increased by the hydrogenation of C_2H_2 ($C_2H_2 + H_2 = C_2H_4$) when the H_2 mole fraction increases.

The larger consumption of OH radicals by H_2 leads to a large increase in H_2O production. H_2O production is almost doubled in the DCPR model when the H_2 initial mole fraction is increased from 16 to 32% and increased by a factor of 10 in the Konnov's model prediction.

In the GRImech mechanism, the OH radicals are mainly consumed by H_2. The OH radicals are slowly consumed by the C_2 species (accumulation of C_2H_2). The large decrease of OH radicals due to their almost exclusive consumption by H_2 has few effects on the CH_4 conversion rate in the GRImech mechanism. The reactions of OH addition onto C_2H_2 involve very minor channel in all cases, for high or low H_2 mole fractions. CH_4 conversion rate is thus not sensitive to the modification of this minor channel in the GRImech mechanism.

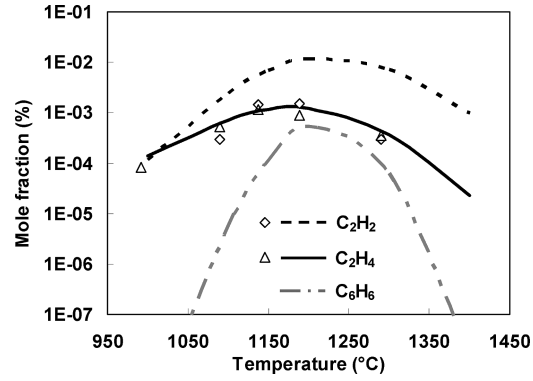

Figure 9. Simulation (lines, DCPR mechanism) and experimental results (points, for C_2H_2 and C_2H_4) of the soot precursors mole fraction as a function of temperature, $\tau = 2$ s, initial gas composition CH_4/7%, H_2O/25%, CO/19%, H_2/16%, CO_2/14%, Ar and N_2 QS.

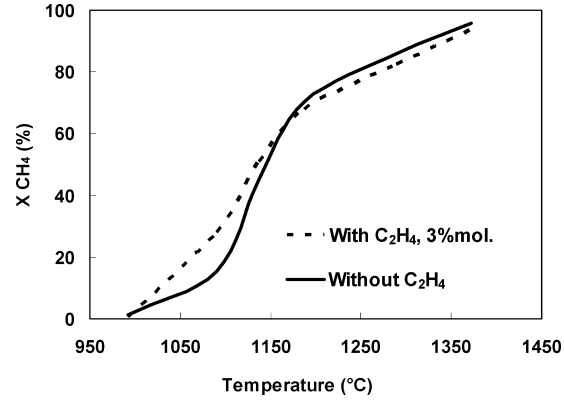

Figure 10. Simulation (DCPR mechanism) of the effect of C_2H_4 on the CH_4 conversion degree as a function of temperature, $\tau = 2$ s, initial gas composition CH_4/14%, H_2O/25%, CO/19%, H_2/16%, CO_2/14%, N_2 QS.

Concerning the effect of initial H_2O mole fraction on the CH_4 conversion, the three mechanisms exhibit about the same predictions (see Figure 5). Indeed, the initial H_2O mole fraction has little effect on CH_4 conversion because the OH radicals are mainly produced at 1200 °C by $CO_2 + H$ due to the high concentration of CO_2 under our conditions. OH radicals concentration is thus relatively independent of H_2O concentration. Though H_2O has very few chemical effects under our conditions, H_2O could exhibit experimentally a thermal effect due to its high thermal capacity, thus leading to better isothermal conditions in the reactor and to a lower soot formation.

6.4. Soot Precursors. It is now well-established that C_2H_2 is one of the main soot precursors.[46,47] The three mechanisms predict a maximum mole fraction of C_2H_2 at 1200 °C (not shown), which is in agreement with numerous gas combustion studies.[47] It was shown that soot formation could be estimated by monitoring the benzene mole fraction in some premixed flames.[48]

Since the DCPR mechanism includes soot precursors, such as benzene, formation, and conversion, C_2H_2, C_2H_4, and benzene mole fractions were simulated with this model and compared with experimental data for C_2H_2 and C_2H_4 (Figure 9). The experimental mole fractions of benzene were unfortunately not available.

The maximum mole fractions for C_2H_2, C_2H_4, and C_6H_6 are obtained for the same temperature (1200 °C). The prediction of C_2H_4 mole fractions is in agreement with the experimental

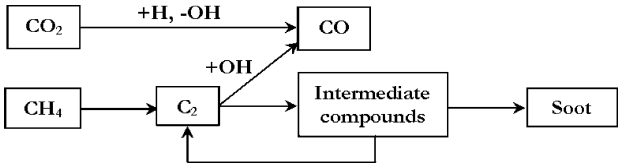

Figure 11. Simplified reaction pathways for the thermal decomposition of CH_4 in a syngas.

mole fractions, whereas C_2H_2 mole fractions are overestimated by the DCPR mechanism (see Figure 9). Future works should deal with the improvement of mechanisms for soot precursors predictions under the conditions of a syngas thermal reforming. Benzene and soot are formed by unsaturated compounds and by secondary tar in the case of a real biomass syngas.[49,50] Complementary studies are needed to understand soot formation mechanisms in a real biomass syngas and to precise the conditions which minimize soot formation.

6.5. Effect of C_2H_4. The reconstituted syngas used during this study did not contain tar, C_2, or other compounds which are produced by the pyrolysis of solid fuels and which could impact the CH_4 conversion. The effect of a compound present in a real syngas was investigated by using C_2H_4 as a surrogate. Figure 10 displays the effect (simulated with the DCPR mechanism) of C_2H_4 on the CH_4 conversion degree.

The presence of 3 mol % of C_2H_4 increases the CH_4 conversion at temperatures lower than 1150 °C. The production of H radicals is favored by H-abstraction to give C_2H_3. C_2H_3 yields another H atom and C_2H_2, whereas CH_3 radicals mainly lead to the formation of C_2H_6 and of CH_4 ($CH_3 + H_2 = CH_4 + H$). The addition of C_2H_4 involves then a larger concentration of H radicals at low temperature which favors the CH_4 conversion ($CH_4 + H = CH_3 + H_2$) and other propagation reactions. The effect of C_2H_4 decreases when the H_2 initial mole fraction increases (not shown). Indeed, H_2 has an inhibiting effect on C_2H_4 conversion due to a shift of the equilibrium of the C_2H_2 hydrogenation ($C_2H_2 + H_2 = C_2H_4$).

7. Conclusion

The aim of this work was to determine the kinetics of the thermal decomposition of CH_4 in a reconstituted syngas and to understand the elementary pathways.

For this purpose, the thermal decomposition of methane was studied in a tubular reactor at a total pressure of 130 kPa, a gas residence time of 2 s, and as a function of temperature (1000−1400 °C), CH_4 (7, 14 vol %), H_2 (16, 32 vol %), and H_2O (15, 25, 30 vol. %) initial mole fractions.

It was shown that the global decomposition rate of CH_4, r (mol m^{-3} s^{-1}), can be described by the following expression:

$$r = \left(4.7 \times 10^7 \exp\frac{-211000}{RT}\right) P_{CH_4}{}^{1.48} P_{H_2}{}^{-0.91} P_{H_2O}{}^{-0.11}$$

The results clearly indicate that temperatures above 1300 °C at a residence time of 2 s are necessary to convert more than 80% of methane.

To identify the main elementary reactions of CH_4 decomposition in our operating conditions, three detailed mechanisms developed for CH_4 combustion were used. The three mechanisms exhibit good agreement as to the effect of the temperature on the CH_4 conversion. The flow rate analyses simulated by the three mechanisms were compared in order to derive the main pathways of CH_4 conversion involved in our experimental conditions.

The three mechanisms lead to the same overall reaction scheme of thermal conversion of CH_4 in the presence of H_2, H_2O, and CO_2 (Figure 11).

Minor channels involve the "direct" oxidation of CH_4 or CH_3 radicals in our conditions. The oxidation of carbon occurs mainly by the addition of OH radicals on C_2 species. OH radicals are mainly produced by CO_2 ($CO_2 + H = CO + OH$). The inhibiting role of H_2 on methane decomposition is explained by a competition between the different OH radicals consumption channels ($H_2 + OH = H_2O + H$). H_2O involves few chemical effects due to the high concentration of CO_2 which mainly controls the OH radicals production. The effect of C_2H_4, as a surrogate of heavier hydrocarbons in the syngas, was simulated. The effect on methane conversion and soot formation of other compounds also present in a syngas produced by biomass pyrolysis such as C_2, tar, and N and S compounds (etc.) has still to be studied.

Literature Cited

(1) Spath, P.; Aden, A.; Eggeman, T.; Ringer, M.; Wallace, B.; Jechura J. *Biomass to Hydrogen Production Detailed Design and Economics Utilizing the Battelle Columbus Laboratory Indirectly-Heated Gasifier*; Technical Report NREL/TP-510-37408, National Renewable Energy Laboratory, 2005; p 161.

(2) Papadopoulo, M.; Normand, S.; Dufour, A.; Muller, T. Evaluation of hydrogen production from biomass gasification. *2nd European Hydrogen Energy Conference*, Zaragoza, Spain, November 22–25, 2005.

(3) Dufour, A.; Girods, P.; Masson, E.; Rogaume, Y.; Zoulalian, A. Synthesis gas production by biomass pyrolysis: effect of reactor temperature on product distribution. *Int. J. Hydrogen Energy* **2009**, *34*, 1726.

(4) Courson, C.; Makaga, E.; Petit, C.; Kiennemann, A. Development of Ni catalysts for gas production from biomass gasification. Reactivity in steam- and dry-reforming. *Catal. Today* **2000**, *63*, 427.

(5) Swierczynski, D.; Courson, C.; Bedel, L.; Kiennemann, A.; Guille, J. Characterization of Ni-Fe/MgO/olivine catalyst for fluidized bed steam gasification of biomass. *Chem. Mater.* **2006**, *18*, 4025.

(6) Nishikawa, J.; Nakamura, K.; Asadullah, M.; Miyazawa, T.; Kunimori, K.; Tomishige, K. Catalytic performance of $Ni/CeO_2/Al_2O_3$ modified with noble metals in steam gasification of biomass. *Catal. Today* **2008**, *131*, 146.

(7) Corella, J.; Orio, A.; Aznar, P. Biomass gasification with air in fluidized bed: Reforming of the gas composition with commercial steam reforming catalysts. *Ind. Eng. Chem. Res.* **1998**, *37*, 4617.

(8) Bain, R. L.; Dayton, D. C.; Carpenter, D. L.; Czernik, S. R.; Feik, C. J.; French, R. J.; Magrini-Bair, K. A.; Phillips, S. D. Evaluation of catalyst deactivation during catalytic steam reforming of biomass-derived syngas. *Ind. Eng. Chem. Res.* **2005**, *44*, 7945.

(9) Torres, W.; Pansare, S. S.; Goodwin, J. G., Jr. Hot gas removal of tars, ammonia and hydrogen sulfide from biomass gasification gas. *Catal. Rev. Sci. Eng.* **2007**, *49*, 407.

(10) Dufour, A.; Celzard, A.; Ouartassi, B.; Broust, F.; Fierro, V.; Zoulalian, A. Effect of micropores diffusion on kinetics of CH_4 decomposition over a wood-derived carbon catalyst. *Appl. Catal., A* **2009**, *360*, 120.

(11) Khan, M. S.; Crynes, B. L. Survey of recent methane pyrolysis literature. *Ind. Eng. Chem.* **1970**, *62*, 54.

(12) Back, M. H.; Back, R. A. Thermal decomposition and reactions of methane. *Pyrolysis: Theory and Industrial Practice*; Albright, L. F., Crynes, B. L., Corcoran, W. H., Eds.; Academic Press: New York, 1983.

(13) Billaud, F.; Baronnet, F.; Freund, E.; Busson, C.; Weill, J. Thermal decomposition of methane. *Rev. Inst. Fr. Pét.* **1989**, *44*, 813.

(14) Kassel, L. S. The thermal decomposition of methane. *J. Am. Chem. Soc.* **1932**, *54*, 3949.

(15) Germain, J. E.; Vaniscotte, C. Craquage du méthane dans un réacteur tubulaire II. Effets de dilution. *Bull. Soc. Chim. Fr.* **1958**, *3*, 319.

(16) Skinner, G. B.; Ruehrwein, R. A. Shock tube studies of the pyrolysis and oxidation of methane. *J. Phys. Chem.* **1959**, *63*, 1736.

(17) Kunugi, T.; Tamura, T.; Naito, T. New acetylene process uses hydrogen dilution. *Chem Eng. Prog.* **1961**, *57*, 43.

(18) Eisenberg, B.; Bliss, H. Kinetics of methane pyrolysis. *Chem. Eng. Prog. Symp. Ser.* **1967**, *72*, 3.

(19) Palmer, H. B.; Lahaye, J.; Hou, K. C. On the kinetics and mechanism of the thermal decomposition of methane in a flow system. *J. Phys. Chem.* **1968**, *72*, 348.

(20) Chen, C. J.; Back, M. H.; Back, R. A. The thermal decomposition of methane. II. Secondary reactions, autocatalysis, and carbon formation; non-Arrhenius behaviour in the reaction of CH3* with ethane. *Can. J. Chem.* **1976**, *54*, 3175.

(21) Billaud, F.; Baronnnet, F.; Guéret, C. P. Thermal coupling of methane in a tubular reactor: parametric study. *Ind. Eng. Chem. Res.* **1993**, *32*, 1549.

(22) Bruggert, M.; Hu, Z.; Huttinger, K. J. Chemistry and kinetics of chemical vapor deposition of pyrocarbon VI. influence of temperature using methane as a carbon source. *Carbon* **1999**, *37*, 2021.

(23) Holmen, A.; Rokstad, O. A.; Solbakken, A. High-temperature pyrolysis of hydrocarbons. 1. Methane to acetylene. *Ind. Eng. Chem. Process Des. Dev.* **1976**, *15*, 439.

(24) Ranzi, E.; Dente, M.; Costa, A.; Bruzzi, V. Thermal decomposition of methane: a mechanistic kinetic scheme. *Chim. Ind.* **1988**, *70*, 1.

(25) Guéret, C.; Billaud, F. Thermal couling of methane: Influence of hydrogen at 1330°C. Experimental and simulated results. *J. Anal. Appl. Pyrol.* **1994**, *29*, 183.

(26) Olsvik, O.; Billaud, F. Thermal coupling of methane. A comparison between kinetic model data and experimental data. *Thermochim. Acta* **1993**, *232*, 155.

(27) Liu, F.; Guo, H.; Smallwood, G. J.; Gülder, O. L. The chemical effect of carbon dioxyde as an additive in an ethylene diffusion flame: implications for soot and NOx formation. *Combust. Flame* **2001**, *125*, 778.

(28) Glarborg, P.; Bentzen, L. L. B. Chemical effects of a high CO_2 concentration in oxy-fuel combustion of methane. *Energy Fuels* **2008**, *22*, 291.

(29) Ranzi, E.; Sogaro, A.; Gaffuri, P.; Pennati, G.; Faravelli, T. A wide range modeling study of methane oxidation. *Combust. Sci. Technol.* **1994**, *96*, 279.

(30) Barbé, P.; Battin-Leclerc, F.; Côme, G. M. Experimental and modeling study of methane and ethane oxidation between 773 and 1573 K. *J. Chim. Phys.* **1995**, *92*, 1666.

(31) Turbiez, A.; Desgroux, P.; Pauwels, J. F.; Sochet, L. R.; Poitou, S.; Perrin, M. GDF-kin®: a new step towards a detailed kinetic mechanism for natural gas combustion modelling. *Proceedings of the IV International Gas Research Conference*, San Diego, CA, November 8–11, 1998; p 371.

(32) Petersen, E.; Davidson, D.; Hanson, R. Kinetics modeling of shock-induced ignition in low-dilution CH_4/O_2 mixtures at high pressures and intermediate temperatures. *Combust. Flame* **1999**, *117*, 272.

(33) Hidaka, Y.; Sato, K.; Henmi, Y.; Tanaka, H.; Inami, K. Shock-tube and modeling study of methane pyrolysis and oxidation. *Combust. Flame* **1999**, *118*, 340.

(34) Coppens, F. H. V.; De Ruyck, J.; Konnov, A. A. The effects of composition on the burning velocity and nitric oxide formation in laminar premixed flames of $CH_4 + H_2 + O_2 + N_2$. *Combust. Flame* **2007**, *149*, 409 (Detailed reaction mechanism for small hydrocarbons combustion. Release 0.5, (2000), available as electronic Supplementary material with the article above).

(35) Smith, G. P.; Golden, D. M.; Frenklach, M.; Moriarty, N. W.; Eiteneer, B.; Goldenberg, M.; Bowman, C. T.; Hanson R. K.; Song, S.; Gardiner, W. C., Jr.; Lissianski, V. V.; Qin, Z. http://www.me.berkeley.edu/gri_mech/, accessed May 15, 2009.

(36) Jönsson, O. Thermal cracking of tars and hydrocarbons by addition of steam and oxygen in the cracking zone. *Fundamental of Thermochemical Biomass Conversion*; Overend, R. P., Milne, T. A., Mudge, L. K., Eds.; Elsevier: London, 1985.

(37) Valin, S.; Castelli, P.; Thiery, S.; Cances, J.; Dufour, A.; Boissonnet, G.; Spindler, B. Upgrading biomass pyrolysis gas by conversion of methane at high temperature: Experiments and modelling. *Fuel* **2009**, *88*, 834.

(38) Morley, C. *Gaseq 0.79*; A Chemical Equilibrium Program for Windows, 2005; http://www.arcl02.dsl.pipex.com/.

(39) Fournet, R.; Baugé, J. C.; Battin-Leclerc, F. Experimental and modeling of oxidation of acetylene, propyne, allene and 1,3-butadiene. *Int. J. Chem. Kinet.* **1999**, *31*, 305.

(40) Belmekki, N.; Glaude, P. A.; Da Costa, I.; Fournet, R.; Battin-Leclerc, F. Experimental and modeling study of the oxidation of 1-butyne and 2-butyne. *Int. J. Chem. Kinet.* **2002**, *34*, 172.

(41) Gueniche, H. A.; Glaude, P. A.; Dayma, G.; Fournet, R.; Battin-Leclerc, F. Rich premixed laminar methane flames doped by light unsaturated hydrocarbons. *Combust. Flame* **2006**, *146*, 620.

(42) Borisov, A. A.; Dragalova, E. V.; Zamanskii, V. M.; Lisyanskii, V. V.; Skachkov, G. I. Kinetics and mechanism of methane self-ignition. *Khim. Fizika* **1982**, *4*, 536.

(43) Borisov, A. A.; Zamanskii, V. M.; Konnov, A. A.; Skachkov, G. I. Mechanism of high-temperature acetaldehyde oxidation. *Sov. J. Chem. Phys.* **1990**, *6*, 748.

(44) Baulch, D. L.; Cobos, C. J.; Cox, R. A.; Frank, P.; Hayman, G.; Just, T.; Kerr, J. A.; Murrells, T.; Pilling, M. J.; Troe, J.; Walker, R. W.; Warnatz, J. Summary table of evaluated kinetic data for combustion modeling. *Combust. Flame* **1994**, *98*, 59.

(45) Kee, R. J.; Rupley, F. M.; Miller, J. A. *CHEMKIN II*; Sandia Laboratories report S 89-8009B, **1993**.

(46) Berthelot, M. Sur la Formation des Carbures Pyrogénés. *Ann. Chim. Phys.* **1869**, *16*, 143.

(47) Richter, H.; Howard, J. B. Formation of polycyclic aromatic hydrocarbons and their growth to soot—a review of chemical reaction pathways. *Prog. Energy Combust. Sci.* **2000**, *26*, 565.

(48) Roesler, J. F.; Martinot, S.; McEnally, C. S.; Pfefferle, L. D.; Delfau, J. L.; Vovelle, C. Investigating the role of methane on the growth of aromatic hydrocarbons and soot in fundamental combustion processes. *Combust. Flame* **2003**, *134*, 249.

(49) Evans, R. J.; Milne, T. A. Molecular characterization of the pyrolysis of biomass. 1. Fundamentals. *Energy Fuels* **1987**, *1*, 123.

(50) Fitzpatrick, E. M.; Jones, J. M.; Pourkashanian, M.; Ross, A. B.; Williams, A.; Bartle, K. D. Mechanistic Aspects of Soot Formation from the Combustion of Pine Wood. *Energy Fuels* **2008**, *22*, 3771.

Received for review March 2, 2009
Revised manuscript received May 16, 2009
Accepted May 22, 2009

IE900343B